Analysis of the Dominant Mode of Convectively Coupled Kelvin Waves in the West African Monsoon

FLORE MOUNIER

LMD/IPSL, CNRS, École Polytechnique, Palaiseau, France

GEORGE N. KILADIS

Physical Sciences Division, NOAA/ESRL, Boulder, Colorado

SERGE JANICOT

LOCEAN/IPSL, IRD, Université Pierre et Marie Curie, Paris, France

(Manuscript received 18 November 2005, in final form 9 August 2006)

ABSTRACT

The dominant mode of convectively coupled Kelvin waves has been detected over the Atlantic and Africa during northern summer by performing composite analyses on observational fields based on an EOF reconstructed convection index over West Africa. Propagating eastward, many waves originate from the Pacific sector, interact with deep convection of the marine ITCZ over the Atlantic and the continental ITCZ over West and central Africa, and then weaken over East Africa and the Indian Ocean. It has been shown that they are able to modulate the life cycle and track of individual westward-propagating convective systems. Their mean kinematic characteristics comprise a wavelength of 8000 km, and a phase speed of 15 m s^{-1}, leading to a period centered on 6 to 7 days. The African Kelvin wave activity displays large seasonal variability, being highest outside of northern summer when the ITCZ is close to the equator, facilitating the interactions between convection and these equatorially trapped waves. The convective and dynamical patterns identified over the Atlantic and Africa show some resemblance to the theoretical equatorially trapped Kelvin wave solution on an equatorial β plane. Most of the flow is in the zonal direction as predicted by theory, and there is a tendency for the dynamical fields to be symmetric about the equator, even though the ITCZ is concentrated well north of the equator at the full development of the African monsoon. In the upper troposphere and the stratosphere, the temperature contours slope sharply eastward with height, as expected from an eastward-moving heat source that forces a dry Kelvin wave response. It is finally shown that the mean impact of African Kelvin waves on rainfall and convection is of the same level as African easterly waves.

1. Introduction

The central and West African region depends heavily on rainfall during the summer monsoon season (Hastenrath 1995). Anticipating the evolution of rainfall throughout the monsoon season would be greatly beneficial to water resources and agricultural and medical efforts over the region. A large amount of work has already been completed on rainfall variability through studies of mesoscale convective systems (MCSs; Laing and Fritsch 1993, 1997; Hodges and Thorncroft 1997; Mathon and Laurent 2001), synoptic-scale easterly waves (Reed et al. 1977; Thompson et al. 1979; Duvel 1990; Thorncroft and Hoskins 1994a,b; Diedhiou et al. 1999; Kiladis et al. 2006; Hall et al. 2006), intraseasonal time-scale variability (Kiladis and Weickmann 1997; Janicot and Sultan 2001; Grodsky and Carton 2001; Sultan et al. 2003; Matthews 2004; Mounier and Janicot 2004), and interannual and decadal time scales (Lamb 1978a,b; Newell and Kidson 1984; Folland et al. 1986; Rowell et al. 1995; Ward 1998; Janicot et al. 2001; Rowell 2001; Grist and Nicholson 2001).

Easterly waves have been identified as fundamental

Corresponding author address: Dr. Serge Janicot, LOCEAN/IPSL, Université Pierre et Marie Curie, Boite 100, 4 Place Jussieu, 75252 Paris CEDEX 5, France.
E-mail: jslod@lodyc.jussieu.fr

DOI: 10.1175/JCLI4059.1

synoptic weather systems in the West African summer monsoon. They are westward-traveling waves originating west of 20°E, developing through barotropic and baroclinic conversions of energy from the African easterly jet (AEJ) located at 600 hPa. Their wavelength varies between 2000 and 4000 km with a westward speed of about 8 m s^{-1}, leading to spectral periodicities between 3 and 5 days. Observations and modeling studies also show significant interactions between these synoptic-scale waves and convection (Duvel 1990; Diedhiou et al. 1999), whose individual MCSs also propagate westward.

Other atmospheric systems exist on synoptic time scales in the Tropics. Convectively coupled equatorial waves have been shown to account for a substantial amount of organization of tropical rainfall (Gruber 1974; Zangvil 1975; Takayabu 1994; Pires et al. 1997; Wheeler and Kiladis 1999, hereafter WK99; Wheeler et al. 2000, hereafter WKW00). For instance, Straub and Kiladis (2002, 2003, hereafter SK02 and SK03) show that Kelvin waves are primary modulators of convective activity within the Pacific ITCZ, and that their structures resemble theoretical Kelvin waves. These equatorially trapped waves organize mesoscale convective elements into larger-scale structures within the Tropics, and as such they might represent a key element in the evolution of convection in the African monsoon. Wang and Fu (2007) studied Kelvin waves reaching central Africa from the Atlantic during northern spring, while Mekonnen (2006) presented preliminary results of the detection of Kelvin waves crossing West Africa during northern summer. Matthews (2004) showed also that the Madden–Julian oscillation (MJO) has a large-scale influence on overall African monsoon activity. However not much is known about the potential influence of these convectively coupled waves on African rainfall variability.

The objective of this paper is to provide evidence of the existence of convectively coupled Kelvin waves modulating convection in the west and central summer monsoon season. The main mode of Kelvin wave will be extracted by an EOF analysis, and its three-dimensional atmospheric structure will be detailed. Its impact on convection will also be compared with those of the African easterly waves. This paper is organized as follows. The datasets used in this study are detailed in section 2. Section 3 presents the detection of convectively coupled Kelvin waves and their impact on convection over the Atlantic and West and Central Africa during northern summer. Section 4 focuses on the dynamics associated with African convectively coupled Kelvin waves and their similarities with the theoretical structure of Kelvin waves. In section 5, the impact of Kelvin waves on statistics of individual African MCSs is shown and is also illustrated in a particular case study. Discussion and conclusions are given in section 6.

2. Datasets

a. The NCEP–DOE AMIP-II Reanalysis

The National Centers for Environmental Prediction (NCEP) and the National Center for Atmospheric Research (NCAR) have completed a reanalysis project with a current version of the Medium Range Forecast (MRF) model (Kalnay et al. 1996). This dataset is a reanalysis of the global observational network of meteorological variables (wind, temperature, geopotential height, humidity on pressure levels, surface variables, and flux variables like precipitation rate) with a "frozen" state-of-the-art analysis and forecast system at a triangular spectral truncation of T62 to perform data assimilation throughout the period 1948 to present. Data are reported on a 2.5° × 2.5° grid every 6 h (00.00, 06.00, 12.00, and 18.00 UTC), on 17 pressure levels from 1000 to 10 hPa, which are adequate resolutions for studying synoptic weather systems. The NCEP–Department of Energy (DOE) Atmospheric Modeling Intercomparison Project II (AMIP-II) Reanalysis (R-2) dataset, the updated version of the NCEP–NCAR reanalysis, has been used here with one value per day by averaging the four outputs of each day. This version of the reanalysis shows significant improvements over the original, especially for land surface parameters and surface–air fluxes (Kanamitsu et al. 2002).

b. The NOAA OLR data

Since 1974, polar orbital Television Infrared Observation Satellite–National Oceanic and Atmospheric Administration (TIROS–NOAA) satellites have established a quasi-complete series of twice-daily measures of outgoing longwave radiation (OLR), at the top of the atmosphere and at a resolution of 2.5° latitude/longitude (Gruber and Krueger 1974). The daily interpolated OLR dataset produced by the Climate Diagnostic Center (Liebmann and Smith 1996) has been used over the period 1979–2000 as a proxy for deep convection. Local hours of the measurements varied during the period 1979–90 between 0230 and 0730 local time in the morning and between 1430 and 1930 in the afternoon. Since deep convection over West Africa has a strong diurnal cycle, a sample of daily OLR based on two values separated by 12 h is obtained to get a daily average. WKW00, SK02, and Roundy and Frank (2004)

have illustrated the utility of OLR in tracing convectively coupled Kelvin waves.

c. The IRD daily rainfall data

To validate the OLR data, a daily interpolated in situ rainfall dataset available from the Institut de Recherches pour le Développement (IRD) has been used (Diedhiou et al. 1999). Daily rainfall amounts at stations located within the West African domain 3°–20°N, 18°W–25°E have been compiled. These data are available for the period 1968–90, including more than 1300 stations from 1968 to 1980, and between 700 and 860 for the period 1981–90. These daily values were interpolated on the same 2.5° × 2.5° grid as NOAA–OLR and NCEP fields, by assigning each station daily value to the nearest grid point and averaging all the values related to each grid point. The greatest density of stations is located between the latitudes 5° to 15°N. Data along 17.5°N can also be taken into account since 30 to 45 stations are available near that latitude.

d. The cloud cluster data

A database identifying cloud clusters from the full-resolution (30 min, 5 × 5 km^2) Meteosat infrared channel (10.5–12.5 μm) has been constructed over the period June–September 1983–99, and MCS identification was carried out through a tracking algorithm based on an areal overlap method (Mathon and Laurent 2001; Mathon et al. 2002). Convective clouds are delineated in Meteosat infrared images using two different brightness temperature thresholds, 233 and 213 K. The 233-K threshold is in the range of the most commonly used thresholds for identifying deep convection (Duvel 1989) and accumulated convective precipitation in the Tropics (Arkin 1979). The 213-K threshold targets the most active part of the convective systems. MCSs have been defined as convective clouds larger than 5000 km^2 at the 233-K threshold. With this definition, they contribute 93% of the total Sahelian cloud coverage at the 233-K threshold for the core of the rainy season, July–September (Mathon et al. 2002). MCSs lasting more than 12 h have been retained and a set of daily duration of MCS occurrences has been built on a 1° × 1° grid. This dataset is available for the monsoon period (June to September) between 1983 and 1999 over the domain 0°–20°N, 60°W–40°E. Because of the varying availability of Meteosat data, the extracted areas are not identical, the overlapping area being 5°N–20°N, 20°W–20°E. No data were available east of 20°E over the period 1989–91, south of 5°N and west of 29°W for the year 1992, and west of 25°W over the period 1993–97.

3. Detection of convectively coupled Kelvin waves

a. Tropics

Figure 1 shows a wavenumber–frequency spectral analysis of the symmetric component of OLR about the equator between 15°N and 15°S for June–September 1979–2000. The shaded spectral peaks lie above roughly the 95% level of significance, and a family of equivalent depth curves for Kelvin, equatorial Rossby (ER), and inertio–gravity waves from shallow-water theory (Matsuno 1966) are also shown (see WK99 for more details). The spectrum reveals the existence of a peak corresponding to the Kelvin wave, lying along equivalent depth curves of around 20–50 m. This corresponds to an eastward phase speed of around 15 m s^{-1}. There is also another peak visible in the spectrum that does not correspond to shallow water modes, in the domain of westward propagating signals between periods 2 and 6 days and zonal wavenumbers 6 to 20. Kiladis et al. (2006) showed that this "TD" signal represents easterly waves in Africa. The boxes in Fig. 1 outline the regions of filtering for the Kelvin and easterly waves examined here, and for ER waves not considered in this paper. Although the Kelvin spectral peak is centered at lower wavenumbers and frequencies than was seen in spectra for the entire year by SK02, we use the same filter as was used in SK02 for consistency, since our results are insensitive to the details of the filtering. The filtering is performed by creating an OLR dataset through an inverse transform that retains only the Fourier coefficients within the designated boxes in Fig. 1 (WK99). Note that the datasets obtained contain the convectively coupled Kelvin wave as well as a significant amount of background convection not organized as Kelvin waves.

b. African convectively coupled Kelvin waves

A spatial EOF (SEOF: see Richman 1986) analysis has been performed for June–September 1979–2000 on Kelvin-filtered OLR values over the domain (10°S–30°N, 80°W–60°E) to account for the potential wavelength of such waves. To determine the number of principal components (PCs) to be retained, the Scree test (Cattell 1966) and the North et al. (1982) rule of thumb were used after taking into account the effect of the autocorrelation on the number of independent data. Following these constraints, PC1/PC2 form an "effectively degenerate multiplet" well separated from PC3 (not shown). PC1 and PC2 represent respectively 8.6% and 8.1% of the filtered total variance. This enables us to focus on the main mode of the Kelvin wave and remove some background signal retained in the filtering procedure.

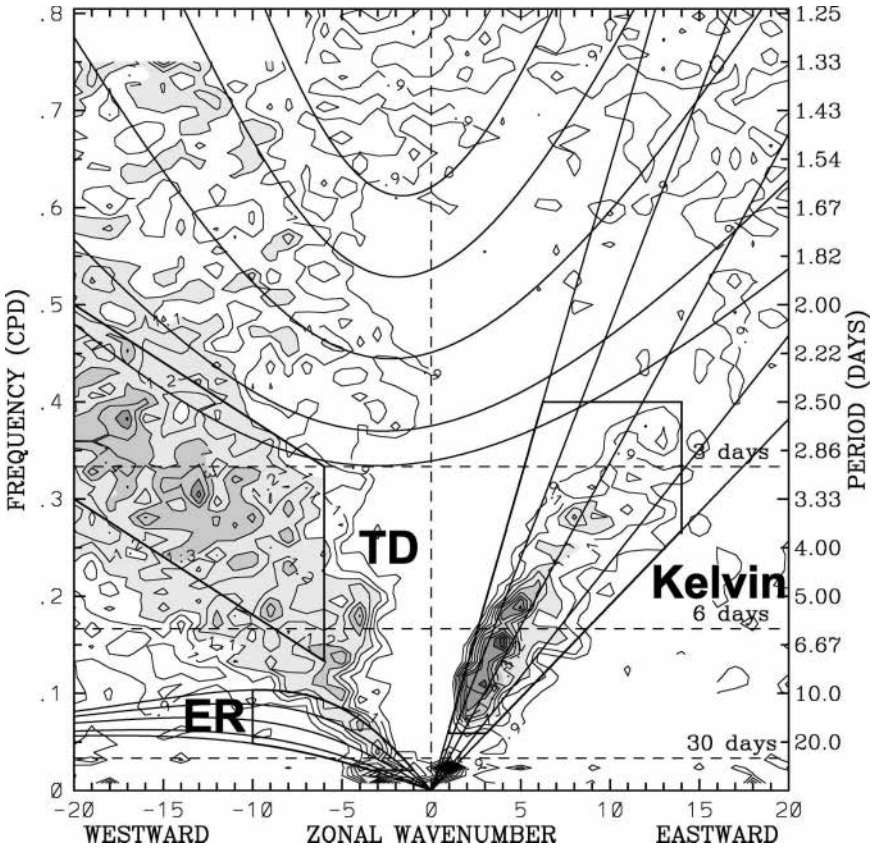

FIG. 1. Regions of wavenumber–frequency filtering calculated for the June–September 1979–2000 records. Contours show the symmetric OLR power divided by a background spectrum (note that the background was calculated for the full 23 yr; see WK99 for details on the computation techniques). Contour interval of this ratio is 0.1 with shading above 1.1 indicative of statistically significant signals. Thick boxes indicate the regions of the wavenumber–frequency domain used for filtering of the OLR dataset to retrieve the longitude–time information of these convectively coupled equatorial waves (Kelvin, equatorial Rossby, and TD). The thin lines are the various equatorial wave dispersion curves for the five different equivalent depths of $h = 8$, 12, 25, 50 and 90 m.

Figures 2a,b shows the two first eigenvectors, which are in spatial quadrature and depict an approximate wavelength of 80° of longitude, or about 8000 km, with highest weights over West Africa and the tropical Atlantic. Figure 2c shows the composite field of Kelvin-filtered OLR (contours) for the difference between the wet and dry Kelvin phase. This has been computed by reconstructing OLR values over the ITCZ area 7.5°–12.5°N, 10°W–10°E using combined SEOF1 and SEOF2 reconstruction ("SEOF12"). We designate a wet (dry) Kelvin phase as a Kelvin wave occurrence over West and central Africa when the reconstructed SEOF12 ITCZ index is negative (positive), meaning higher (weaker) convective activity in the ITCZ. The wet (dry) cases have been selected when the standardized reconstructed ITCZ index is minimum (maximum) and weaker (higher) than minus (plus) 1.5. Similar composite fields for unfiltered rainfall data are also displayed (shaded). The composite fields have been computed using the common period June–September 1979–90 between the NOAA–OLR and the IRD–rainfall datasets. This yields an average of five wet and five dry cases per summer. There are about 10 wet and 10 dry events per summer when we consider a threshold of 1 standard deviation, and about 2 wet and 2 dry cases per summer for a threshold of 2 standard deviations. Positive rainfall anomalies correspond rather well with negative OLR values and vice versa, confirming the interpretation based on OLR. The high range of these OLR and rainfall differences between wet and dry Kelvin phases means that these waves are able to significantly modulate the convective activity in the ITCZ during the summer monsoon. Moreover the spatial extension of the anomalies means that a large part of the

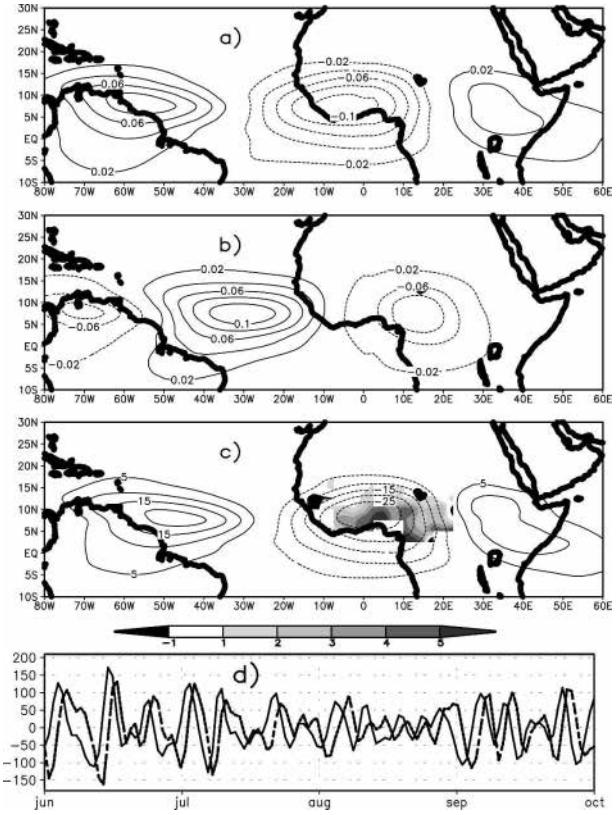

FIG. 2. June–September 1979–90 (a) first and (b) second eigenvectors of the SEOF analysis of Kelvin-filtered OLR. (c) Composite fields of Kelvin-filtered OLR (contours) for the difference between wet and dry Kelvin phases, computed by using the reconstruction of the OLR values over the ITCZ area 7.5°–12.5°N, 10°W–10°E by SEOF1 and SEOF2 (called SEOF12). The wet (dry) cases have been selected when the standardized reconstructed OLR ITCZ index is minimum (maximum) and weaker (higher) than minus (plus) 1.5. Similar composite fields for unfiltered rainfall data are also displayed (shaded). OLR differences are expressed in W m^{-2} and rainfall differences in mm day^{-1}. (d) Time series of PC1 (solid line) and PC2 (dashed line) in summer 1984.

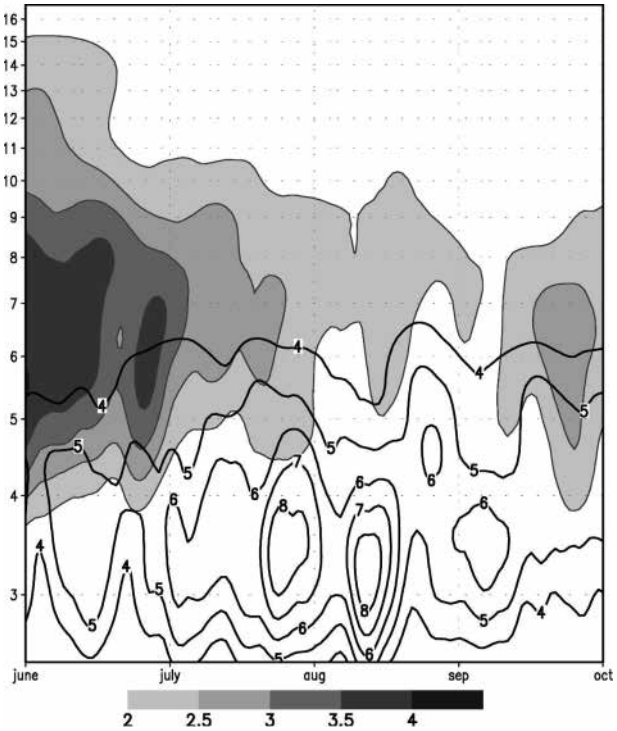

FIG. 3. Mean wavelet diagram performed on indexes computed over the ITCZ area (7.5°–12.5°N, 10°W–10°E) over the period June–September averaged for 1979–2000. Shading denotes the Kelvin-filtered OLR SEOF12 reconstruction index. Contours denote the TD-filtered reconstructed index.

convective activity over West and Central Africa can be influenced by the crossing of such a Kelvin wave (similar SEOF analysis performed on the longitude domain 30°W–30°E provides 16.3% and 15.3% of explained variance for SEOF1 and SEOF2, respectively). Figure 3d shows the PC1 and PC2 time series in summer 1984. This depicts a similar contribution to these two components with weaker weights from mid July to the end of August. These components are in temporal quadrature and have a periodicity between 6 and 8 days. We will see in the following that this is associated with an eastward propagating signal, confirming the identification of Kelvin waves modulating the mean convection over the African monsoon domain, since its spatial pattern is superimposed on the climatological mean location of the ITCZ over Africa.

Figure 3 shows the mean wavelet signal [see Torrence and Compo (1998) for a detailed presentation of the method] from June to September averaged over the years 1979 to 2000 of the Kelvin-filtered OLR SEOF12 reconstructed ITCZ index (shaded) and the TD-filtered reconstruction index (see section 6). This pattern shows large variations during summer with a higher and more periodicity-extended signal in June (from 4 to 15 days), and a weaker signal in August more centered on around 5 to 10 days. In fact the signal is maximized during spring and fall (not shown, see Roundy and Frank 2004) when the ITCZ is close to the equator and has a very active convective activity along the Guinea coast. This may be due to the fact that equatorially trapped Kelvin waves might have less impact on convection when the ITCZ is located farther northward. Based on the wavelet diagrams for the different years, we have examined more precisely the distribution of the periodicities where the Kelvin signal is the highest, both for the different months of the summer and for the different years over 1979–2000. We have also considered the Kelvin signal seen through its dominant mode

TABLE 1. Distribution of the periodicities in days where the wavelet signal from Fig. 3 is the highest by month and for the summers of 1979–2000, for the Kelvin signal seen through its dominant mode (SEOF12) and through the entire filtered signal covering the Kelvin box of Fig. 1. (d denotes days.)

	SEOF12	Kelvin box
Jun	5.9	5.5
Jul	7.3	5 and 6.5
Aug	7.9	4.5
Sep	6.5	5.5
Mean	6.9	5.1 and 5.5
Jun–Sep 1979–2000	6 d for 17 yr 6.5 d for 4 yr 7 d for 1 yr	6 d for 16 yr 4 d for 6 yr

(SEOF12) and through the whole filtered signal covering the Kelvin box of Fig. 1. Table 1 shows first that the dominant Kelvin mode has a periodicity higher than the whole Kelvin signal, 6.9 days versus 5.1–5.5 days, with a seasonal variation leading to higher periods in July–August. The distribution through the 22 summers depicts a dominance of the 6-day periodicity with a small subset of years with higher (lower) periodicities for the dominant Kelvin mode (whole Kelvin box) signal.

4. Convection and dynamics associated with African convectively coupled Kelvin waves

In the following we will consider the composite fields associated to what we call the "dominant mode" of the Kelvin wave activity over Africa, that is, computed using the Kelvin-filtered ITCZ OLR index reconstructed by SEOF12 over the period June–September 1979–2000 on the domain 7.5°–12.5°N, 10°W–10°E. This is referred to as the "Kelvin wave index." Similar computations have been performed based on the entire Kelvin-filtered index (from the Kelvin box of Fig. 1). The results obtained (not shown) are less spatially coherent than for the dominant mode, indicating that use of the entire Kelvin box includes noise unrelated to Kelvin wave activity.

a. The horizontal atmospheric pattern

Figure 4a shows a wet-minus-dry composite sequence associated with the Kelvin wave index over the period June–September 1979–2000. This sequence depicts the Kelvin-filtered OLR (shaded), the nonfiltered 200-hPa divergent wind fields (vectors) and the nonfiltered 200-hPa velocity potential field. It goes from t_0 minus 6 days to t_0 plus 6 days with an irregular lag (days are marked in red in the left corner). The signals presented are significant at the 95% level. The level of significance has been computed with the Student's t test defined locally at each grid point. This sequence reveals that the Kelvin wave signal detected over West and Central Africa is part of a regional-scale phenomenon active between approximately 120°W and 90°E, originating in the east Pacific basin and ending over the Indian Ocean. At 200 hPa (925 hPa; not shown) nonfiltered anomalies of horizontal divergence (convergence), shown in inverse Laplacian form as velocity potential, are collocated with the eastward propagation of a convective envelope. The associated 200-hPa nonfiltered divergent winds exhibit remarkable symmetry about the Kelvin wave OLR signal. On both sides of this structure, weaker convection is associated with oppositely signed perturbations of velocity potential. When the convectively coupled Kelvin wave reaches the east side of the African continent, the atmospheric signal weakens substantially although some remnant of especially the OLR anomaly continues to propagate into the Indian Ocean. The fact that nonfiltered velocity potential anomalies are very consistent with Kelvin-filtered OLR anomalies confirms that over this domain the Kelvin wave has a substantial impact on the mass circulation and convection.

Figure 4b shows the wet-minus-dry composite sequence associated with the same index, for the unfiltered OLR (shaded), the unfiltered 925-hPa wind (vectors), and 925-hPa geopotential fields. This sequence

→

FIG. 4. (a) Composite time sequences based on the Kelvin wave index (computed on the red box). From this standardized index time series, we retained the dates (called t_0) when it is maximum (minimum) and greater (lower) than 1.5 to define a dry (wet) Kelvin phase. The respective wet-minus-dry composite sequences have been computed on June–September 1979–2000 and are shown for the Kelvin-filtered OLR (shaded), the nonfiltered 200-hPa divergent wind fields (vector), and nonfiltered 200-hPa velocity potential field (contours); shown values are significant at the 95% level. These sequences go from $t_0 - 6$ days to $t_0 + 6$ days with an irregular lag (day marked on the left corner). Kelvin-filtered OLR anomalies are expressed in W m^{-2}, velocity potential in 10^6 m^2 s^{-2}, and vector scale (m s^{-1}) is displayed below. (b) As in (a) but the respective wet-minus-dry Kelvin phase composite sequences are shown for nonfiltered OLR (shaded), nonfiltered 925-hPa wind field (vectors), and nonfiltered 925-hPa geopotential field (contours); shown OLR and wind values are significant at the 95% level. These sequences go from $t_0 - 4$ days to $t_0 + 4$ days with a 1-day lag (day marked on the right corner). OLR anomalies are expressed in W m^{-2}, geopotential in mgp, and vector scale (m s^{-1}) is displayed below.

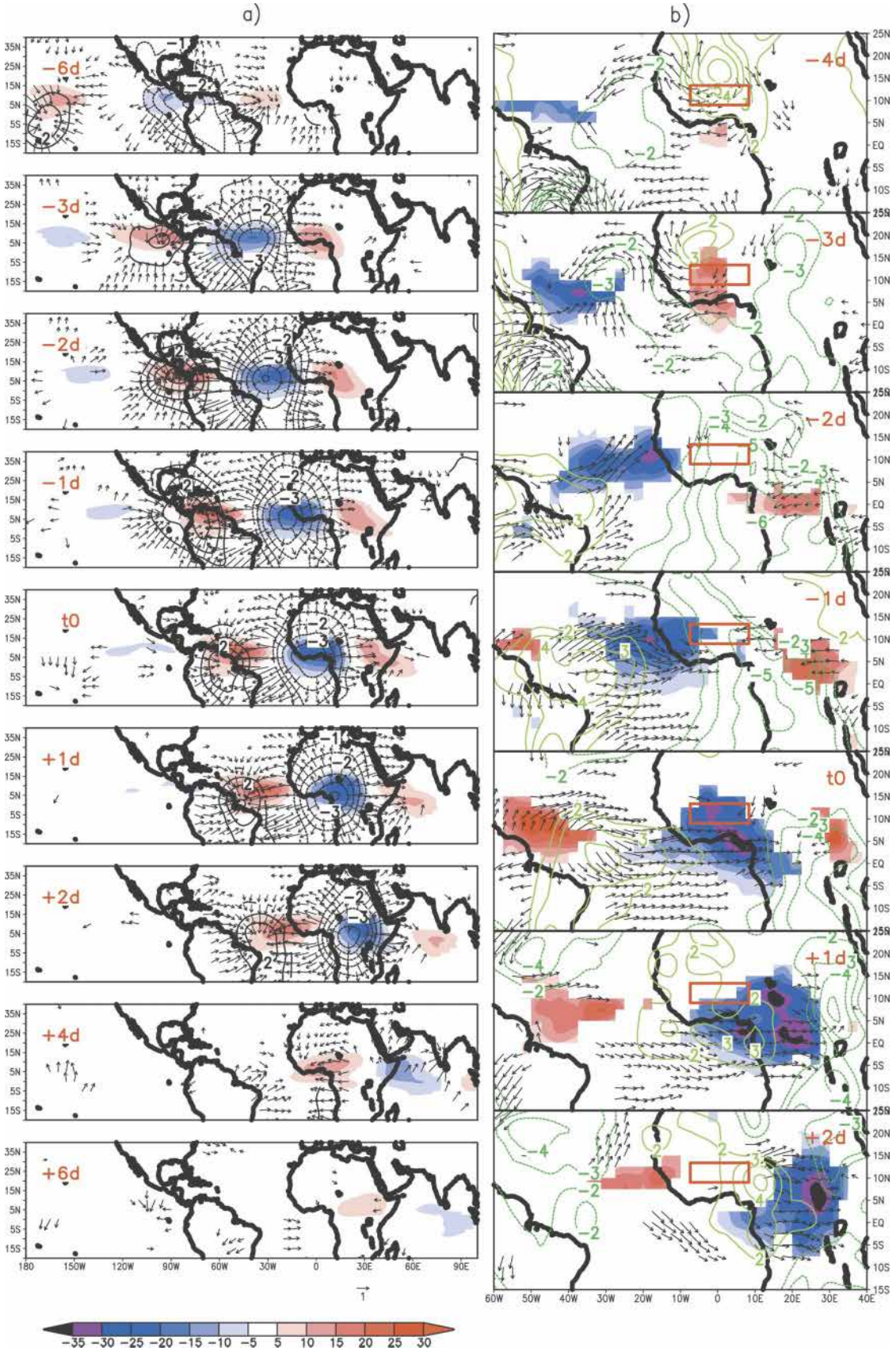
a)
b)
−6d
−3d
−2d
−1d
t0
+1d
+2d
+4d
+6d
−4d
−3d
−2d
−1d
t0
+1d
+2d
−35 −30 −25 −20 −15 −10 −5 5 10 15 20 25 30

goes from $t_0 - 4$ to $t_0 + 2$ days with 1-day lag. The results for OLR and the wind fields are significant at the 95% level. Highly significant unfiltered OLR anomalies confirm that the Kelvin wave shows a non-negligible signal on convection over Africa and the tropical Atlantic. It yields a typical amplitude of the convection modulation of up to 30 W m^{-2} (or about plus or minus 15 W m^{-2} around the mean) associated with this wave activity. The OLR anomaly pattern evolves from being zonally oriented over the Atlantic to having a northwest–southeast tilt over West and central Africa and a meridional orientation over East Africa, consistent with the width of the ITCZ. The near-surface structure shows some resemblance with a theoretical equatorially trapped Kelvin wave solution on an equatorial β plane (Matsuno 1966). As in Kelvin waves over the Pacific (SK02; SK03), the passage of the wave is preceded by easterly and followed by westerly wind anomalies, partly in phase with negative and positive geopotential perturbations, respectively, the whole structure propagating at the same speed. Most of the flow is in the zonal direction as predicted by theory, although the strong monsoonal heating over West Africa does favor meridional southerly inflow. This wind field anomaly pattern leads to an enhancement of inland moisture advection by the zonal flow component, along the Guinean coast and off the Fouta-Djalon orography at the location of the "westerly low-level jet" pointed out by Grodsky et al. (2003). The convergence of westerly and easterly flows contributes then to the enhanced convection over West and central Africa. Also, as in the Pacific (SK02; SK03), there is a tendency for the dynamical fields to be much more symmetric about the equator, with large Southern Hemisphere signals, even though the convection is concentrated well north of the equator, at the latitude of the ITCZ.

To synthesize the kinematic properties of the African Kelvin wave, Fig. 5 shows the wet minus dry composite time–longitude diagram of 7.5°–12.5°N averaged unfiltered OLR (shaded) and mean sea level pressure (MSLP; contours) based as done for previous computations on the Kelvin wave index for the period June–September 1979–2000. The largest part of the OLR signal is located between 50°W and 30°E, up to 30 W m^{-2} (i.e., about ± 15 W m^{-2} around the mean), and the pattern shows a wavelength of 8000 km, an eastward phase speed of 15 m s^{-1}, and a resultant period of 6 days. This phase speed is a characteristic of convectively coupled Kelvin waves observed over the Pacific (SK02; SK03). Only one complete phase of the wave is evident with successively positive, negative, and positive OLR anomalies. West of 60°W, a bit faster and weaker signal is evident that can be traced back to the

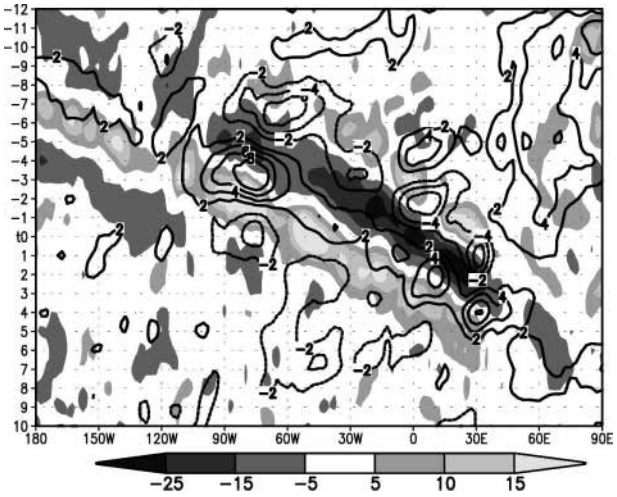

FIG. 5. Composite time–longitude diagram based on the Kelvin wave index for the period June–September 1979–2000. From this standardized index time series, we retained the dates (called t_0) when it is maximum (minimum) and greater (lower) than 1.5 to define a dry (wet) Kelvin phase. The respective wet-minus-dry composite sequences have been computed for the nonfiltered OLR (shaded, W m^{-2}) and nonfiltered MSLP (contours, hPa) averaged over the latitudes 7.5°–12.5°N. This Hovmöller diagram goes from $t_0 - 12$ days to $t_0 + 10$ days over the domain 180°–90°E.

date line. On the other hand, a weak signal reappears around 60°E but without clear propagation. The fact that the Kelvin wave train slows down over the Atlantic and Africa might be an indication of a stronger coupling of the wave to the convection (WKW00). MSLP values on Fig. 5 are in quadrature with the OLR values and propagate eastward at the same speed over the Atlantic and Africa, consistent with the theoretical structure of Kelvin waves and with OLR–geopotential patterns in Fig. 4b. A striking feature is the large stationary negative then positive MSLP anomalies observed over 100°–40°W between $t_0 - 9$ and $t_0 - 2$. When looking at the time sequence of MSLP maps (not shown), it appears that these MSLP anomalies originate from South America at 20°S and propagate northward along the Andes mountain range to reach the equatorial latitudes of the Atlantic basin around 60°W, where they merge with weak pressure anomalies coming from the eastern Pacific. More investigation is needed to better understand whether this signal originates as a response or is an actual forcing of the Kelvin wave over South America.

b. The vertical atmospheric pattern

The vertical structure of the Kelvin wave pattern in a zonal–vertical plane along the mean axis of the ITCZ is presented in Fig. 6. This figure displays the wet-minus-

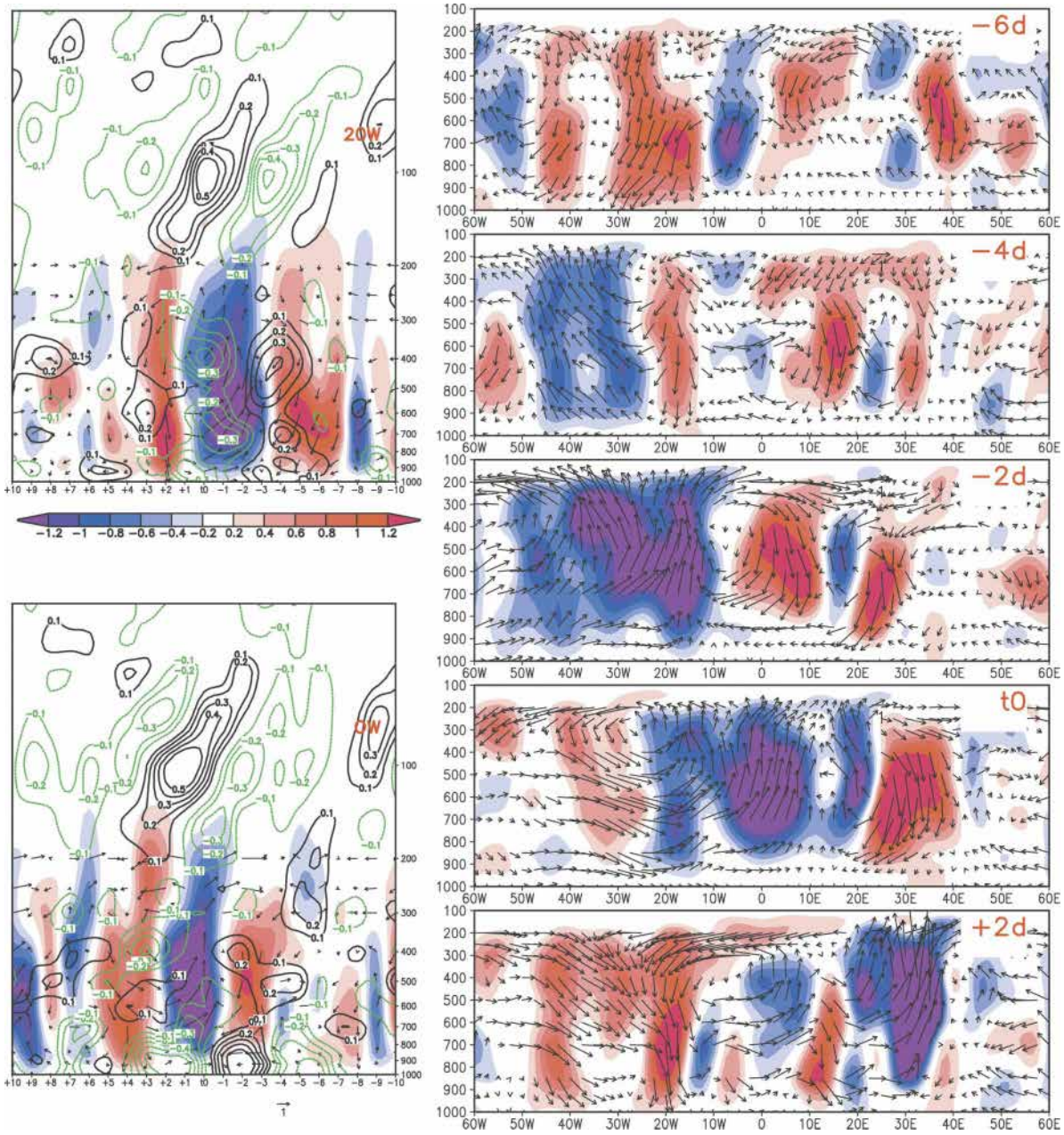

FIG. 6. Similar to Fig. 4 but for wet-minus-dry Kelvin phase composite sequences, averaged between 7.5° and 12.5°N, of unfiltered vertical velocity (shaded, multiplied by 50 and expressed in Pa s^{-1}), zonal/vertical wind (vector), and temperature (contours, black for positive and green for negative values; K) on a zonal–vertical plane. (a) The time evolution between ±10 days at 20°W and 0° longitudes (marked in red in the right corner). (b) The longitude–time evolution between 60°W and 60°E from $t_0 - 6$ to $t_0 + 2$ days with a 2-day lag (marked in red in the right corner).

dry Kelvin phase composite sequences averaged between 7.5° and 12.5°N of unfiltered vertical velocity, zonal/vertical wind, and temperature. In Fig. 6a there are time–height sections (from $t_0 - 10$ to $t_0 + 10$ days) of zonal–vertical motion and temperature at 20°W and 0° extending up to 30 hPa. In Fig. 6b there are zonal cross sections of the zonal–vertical circulation at various time lags, from $t_0 - 6$ when the Kelvin wave is already developed over the Atlantic and the eastern Pacific to $t_0 + 2$ days when it reaches East Africa.

The time sequence of the zonal cross section of the zonal and vertical circulation (Fig. 6b) is also consistent with the passage of a Kelvin wave train. The good correspondence between the location of negative OLR

anomalies (Fig. 4b) and the highest upward velocities provides confidence in the consistency of these results, although the correspondence between positive OLR and downward motion anomalies is not so well defined. The maximum upward motion is about -0.3 cm s^{-1} (taking into account the scale used; see caption). The pattern is the most developed at t_0 with a large area of convection constituted by upward motion between 20°W and 20°E and two areas of downward motion, one to the west between 45° and 25°W and one to the east around 30°E. Upward motion has a peak at 500 hPa between 10°W and 10°E, corresponding to the northwest–southeast axis of the enhanced convective area (Fig. 4b). There is another core between 20° and 15°W that has a peak at 700 hPa corresponding to the enhanced zonal wind along the Guinean highs of Fouta-Djalon in the area of the westerly low-level jet identified by Grodsky et al. (2003). Interestingly, this area corresponds to a genesis location for MCSs (Mathon et al. 2002), which then propagate westward over the tropical Atlantic. This zonal circulation is also well developed at $t_0 - 2$ where the upward motion expands from 50° to 10°W and is closely linked to the subsiding motions ahead between 5°W and 10°E. The size of the circulation cell varies substantially with time with a wide development between $t_0 - 2$ and t_0 and with a less well organized zonal circulation before $t_0 - 2$ and after t_0. These differences might be due to greater interactions with the ITCZ, which is more expanded over West and central Africa than over the Atlantic. However, when considering the panels of Fig. 6a showing the time evolution of the zonal circulation over 20° and 0°W, we can detect a coherent organization of the circulation between $t_0 - 7$ and $t_0 + 3$ at 20°W and between $t_0 - 4$ and $t_0 + 6$ at 0° longitude. This vertical circulation is consistent with the one depicted Kelvin wave over the western Pacific (WKW00; SK03), although the peak upward motion and implied heating field is at 500 hPa, significantly lower than the 300-hPa peak seen over the Pacific. This may reflect a fundamental difference between continental and oceanic convection between the two regions.

Time sections of the vertical temperature profile associated with this circulation are described in Fig. 6b, up to 30 hPa, over the ocean (20°W) and over the continent (0°). In the troposphere, above the ocean at 20°W, two vertical motion anomalies of equal amplitude but opposite sign are evident, the downward leading the upward, and a third one, with weak downward velocity, follows the upward signal. This wave train is then organized as two zonal circulation cells around positive (ahead) and negative (behind) temperature anomaly cores well developed in the troposphere. Positive temperature anomalies lead the convective core, with peaks at about 925 and 400 hPa, and negative temperature anomalies follow the convection. Behind the enhanced upward motion, most of the troposphere is cool, which indicates that on the large scale the latent heating of the moist convection is not sufficient to overcome the adiabatic cooling of the vertical motion. Above the continent (0°), some differences appear within an overall similar pattern. The peak of upward motions is located at 500 hPa instead of 700 hPa over the ocean, and a westward tilt with height is now evident below approximately 500 hPa. Also, the period is shorter, being about 6 days over the continent instead of 8 days over the ocean. Both at 20°W and 0°, within and slightly ahead of the region of deep upward motion, the temperature contours slope sharply eastward with height above 250 hPa and in the stratosphere. This is expected from an eastward-moving heat source, forcing a dry Kelvin response (e.g., WKW00).

Overall, the stratospheric signals are consistent with a vertically propagating Kelvin wave with eastward and downward phase and upward energy propagation. This lower-stratospheric Kelvin wave structure appears to be forced from below by the deep convection. In the troposphere, the quadrature arrangement between vertical motion and temperature, a warm temperature anomaly leading the upward motion (and diabatic heating), and the cold signal following it, is close to the expected dry Kelvin wave pattern. This is also rather consistent with the Kelvin wave patterns observed over the different sectors of the Pacific Ocean and the Indian basin (WKW00; SK02; SK03), although there is no clear westward tilt with height below 250 hPa as observed over these oceanic basins. At 20°W no tilt is evident, while at 0° some westward tilt is present but with a not-so-well-organized pattern. Previous studies suggested that the Kelvin wave dynamical structure is not strongly affected by differences in basic-state winds, as was also demonstrated theoretically by Zhang and Webster (1989). Over the eastern Atlantic and Africa, it is possible that the observed moist Kelvin wave vertical structure results from the background monsoon circulation perturbing the pattern of the theoretical Kelvin wave, whereas the horizontal dynamical fields are less affected, being more characterized by symmetry about the equator.

5. Impact of Kelvin waves on African mesoscale convective systems activity

We now examine more precisely the impact of convectively coupled Kelvin waves on convective activity by considering the high-resolution MCS dataset devel-

oped by Mathon and Laurent (2001). These data are rather consistent with the NOAA OLR data since they are both based on OLR, but some differences exist due to the sampling rate, which is much higher for the MCS and which induces a slight mean time lag in the day, leading to MCS envelopes located a bit eastward of OLR envelopes. Wet-minus-dry composite time sequences of MCS occurrences based on the Kelvin wave index are shown in Fig. 7 for the period June–September 1983–99. Only MCSs lasting more than 12 h have been considered, which are also MCSs with larger mean size (Fig. 6 of Mathon and Laurent 2001). These MCSs contribute to about 75% of their total coverage at the 233-K threshold, which demonstrates the importance of long-lived MCSs in spite of their small occurrence numbers (Fig. 6 of Mathon and Laurent 2001). MCS occurrence is expressed as duration of occurrences per day by 30-min steps (the scale can go then from 0 to 48). Figure 8 shows similar composite sequences but for wet and dry Kelvin phases separately. The time series below Fig. 7 represents the corresponding composite time sequence from $t_0 - 10$ to $t_0 + 10$ days of the mean MCS occurrences averaged over the African ITCZ area 7.5°–12.5°N, 10°W–10°E for wet (solid line) and dry (dashed line) Kelvin phases.

Both Fig. 7 and Fig. 8 show clearly the eastward propagating envelope of the Kelvin wave modulating the mean duration of occurrences of MCSs over the eastern tropical Atlantic as well as West and central Africa. Figure 8 shows that a Kelvin wave can impact convection in the ITCZ by enhancing the westerly wind field south of it and contributing to the expansion of the convective area of the African ITCZ. It shows also that Kelvin waves are able to modulate convective activity over the whole ITCZ domain, and in particular to the south over the Cameroon highlands and Central Africa. This high-resolution dataset enables us to identify high values of maximum MCS occurrence duration, in particular over the Cameroon and off the Fouta-Djalon

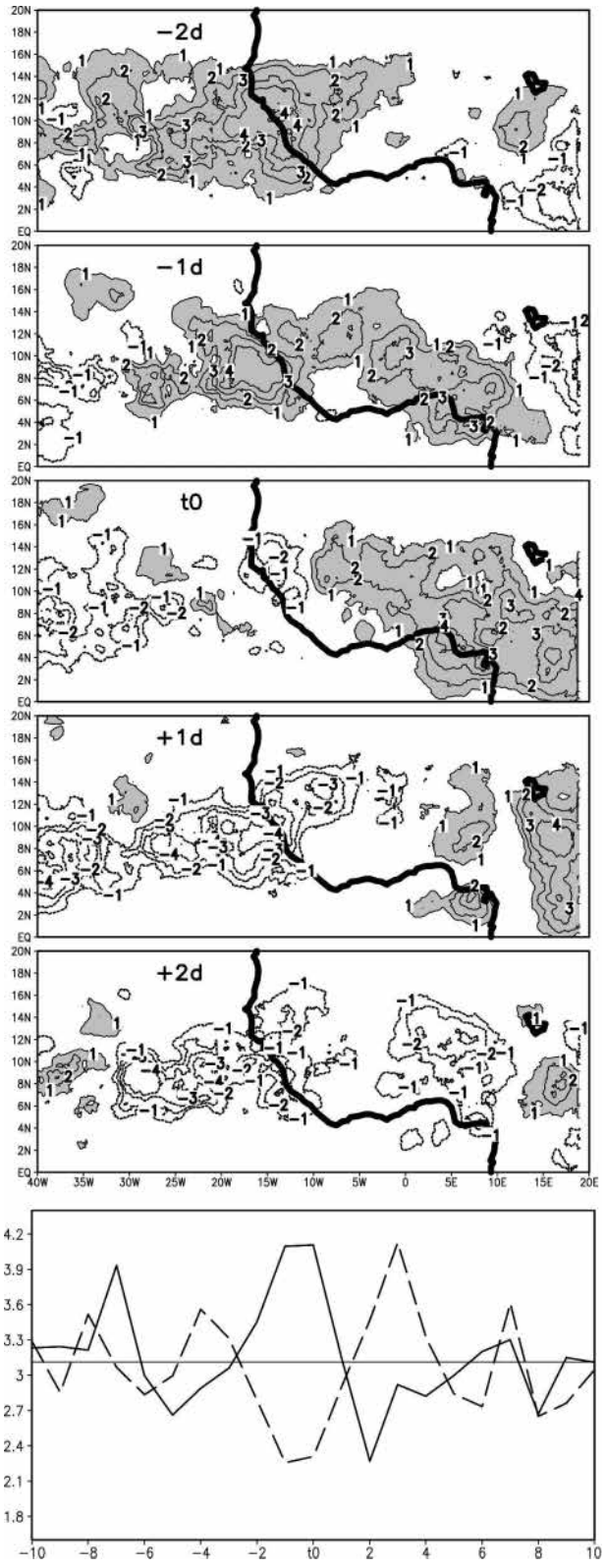

→

FIG. 7. Wet-minus-dry composite time sequence of MCS occurrences at the threshold 233 K based on the Kelvin wave index for the period June–September 1983–99. From this standardized index time series, we retained the dates (called t_0) where it is maximum (minimum) and greater (lower) than 1.5 to define a dry (wet) Kelvin phase. MCS dataset is available over the domain 0°–20°N, 40°W–20°E. MCS occurrence is expressed in duration of occurrences per day by 30-min steps (the scale can go then from 0 to 48) for MCSs lasting more than 12 h (shaded for positive values). The panel below represents the corresponding composite time sequence from $t_0 - 10$ to $t_0 + 10$ days of the mean MCS occurrences averaged over the domain 7.5°–12.5°N, 10°W–10°E for wet (solid line) and dry (dashed line) Kelvin phases.

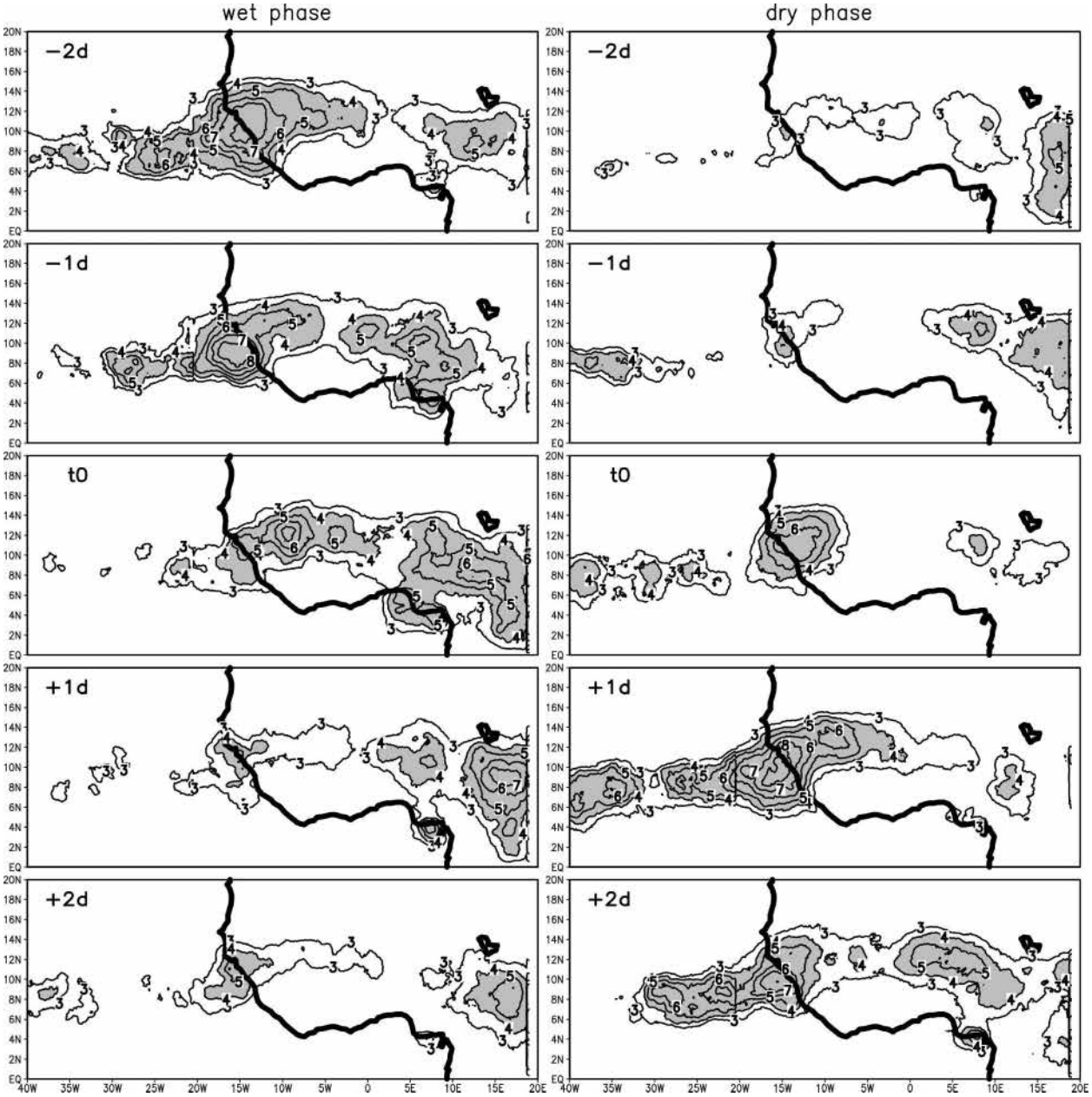

FIG. 8. As in Fig. 7 but for (left) wet and (right) dry Kelvin phases. Only isolines greater or equal than 3 are displayed.

orography. It also demonstrates the high zonal extension of the convective modulation in the ITCZ, and also the break in the ITCZ over West Africa during a dry phase occurrence. The composite time sequence below Fig. 7 indicates that wet and dry Kelvin phases of convection modulation are rather symmetric and correspond to the mean periodicity of 5 to 7 days already seen over Africa. It confirms also that only one complete wave is evident, suggesting that Kelvin-type activity is characterized by the occurrence of separate individual events and not a train of several waves.

Such an example is shown in Fig. 9 between 1 and 10 July 1984. Superimposed on the MCS occurrence duration (shaded), the Kelvin-filtered OLR sequence is represented by contours from the filtered NOAA OLR dataset (Fig. 9a). One wave train is detected and traced on the figure. The modulation of the MCS occurrence duration can be rather well associated with the eastward crossing of the dry and wet phases of the Kelvin wave. The eastward propagating signal of enhanced convection appears as enhanced deep cloudiness composed of smaller spatial and temporal scale MCSs

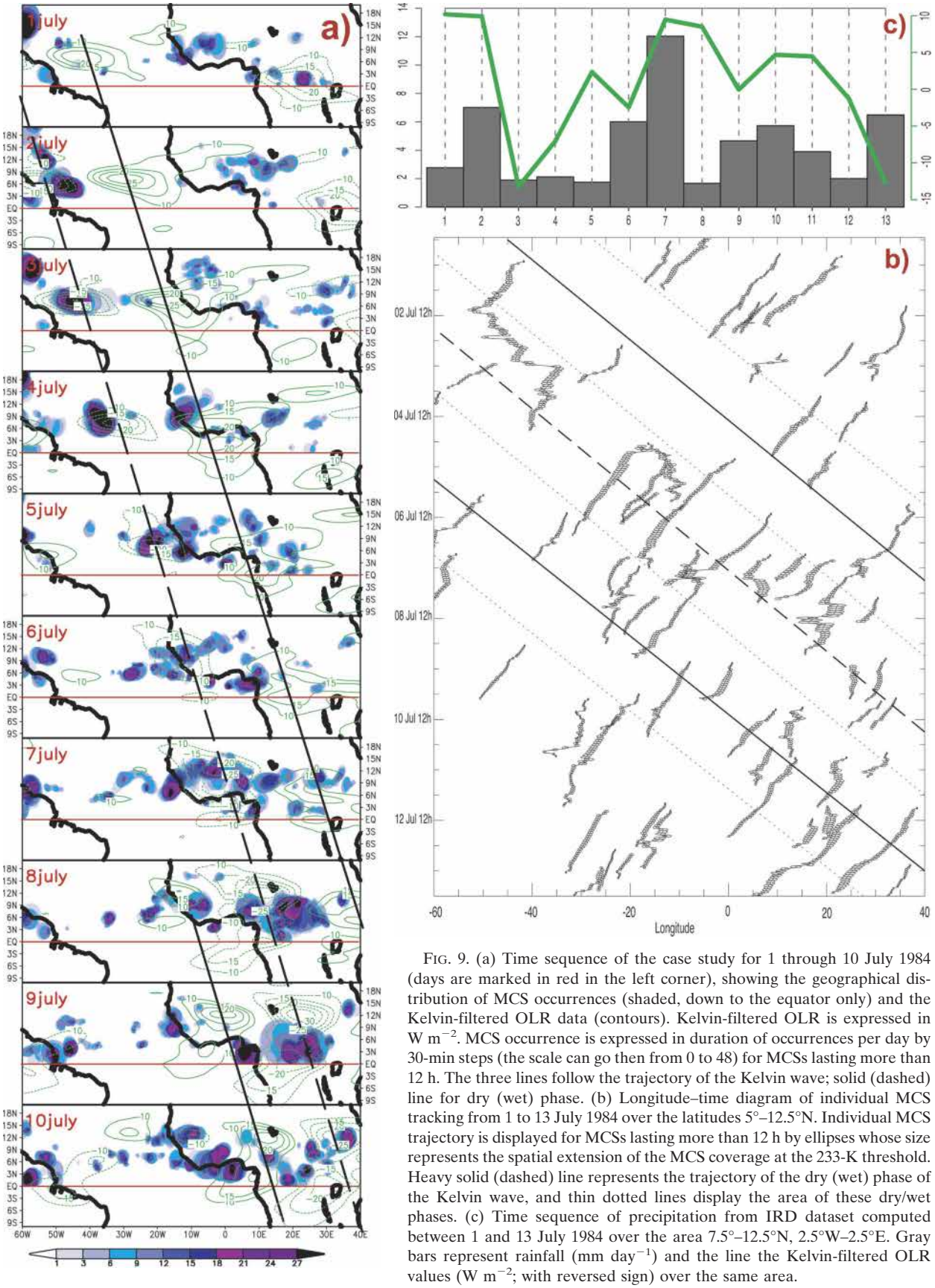

FIG. 9. (a) Time sequence of the case study for 1 through 10 July 1984 (days are marked in red in the left corner), showing the geographical distribution of MCS occurrences (shaded, down to the equator only) and the Kelvin-filtered OLR data (contours). Kelvin-filtered OLR is expressed in W m^{-2}. MCS occurrence is expressed in duration of occurrences per day by 30-min steps (the scale can go then from 0 to 48) for MCSs lasting more than 12 h. The three lines follow the trajectory of the Kelvin wave; solid (dashed) line for dry (wet) phase. (b) Longitude–time diagram of individual MCS tracking from 1 to 13 July 1984 over the latitudes 5°–12.5°N. Individual MCS trajectory is displayed for MCSs lasting more than 12 h by ellipses whose size represents the spatial extension of the MCS coverage at the 233-K threshold. Heavy solid (dashed) line represents the trajectory of the dry (wet) phase of the Kelvin wave, and thin dotted lines display the area of these dry/wet phases. (c) Time sequence of precipitation from IRD dataset computed between 1 and 13 July 1984 over the area 7.5°–12.5°N, 2.5°W–2.5°E. Gray bars represent rainfall (mm day^{-1}) and the line the Kelvin-filtered OLR values (W m^{-2}; with reversed sign) over the same area.

propagating westward and embedded in the Kelvin wave convective envelope. In this case, there is a local enhancement of convection over the Guinea Highlands as the Kelvin wave comes ashore, then another larger enhancement of convection over West Africa and farther east around 20°E as the wave propagates farther inland.

Figure 9b highlights the impact of this Kelvin wave on the MCS life cycle by displaying the corresponding longitude–time diagram of individual MCS tracking over the latitudes 5°–12.5°N. Each individual MCS track is displayed by ellipses whose size represents the spatial extension of the MCS coverage at the 233-K threshold. Heavy solid (dashed) lines represent the track of the dry (wet) phase of the Kelvin wave, and thin dotted lines display the area of these dry/wet phases. This wave travels at about 15 m s^{-1}, as seen for the average composite Kelvin wave. During the first dry phase of the Kelvin wave, there are very few and very weak convective systems. On the other hand, the wet phase occurrence is associated with more and highly developed convective systems. Rather surprisingly we also observe that some of these systems do not have a regular westward trajectory but show some backward (eastward) displacements that may be due to the dynamical forcing of the eastward propagating Kelvin wave. Lastly, when the following dry Kelvin wave occurs, we observe fewer and weaker convective systems than during the wet Kelvin wave phase.

The impact of the Kelvin wave crossing over West Africa on local rainfall is highlighted in Fig. 9c through the time sequence of precipitation from the IRD dataset computed over the area 7.5°–12.5°N, 2.5°W–2.5°E (bars). The Kelvin wave crossing this area is depicted by the Kelvin-filtered OLR values computed over the same area (green line; shown with reversed sign to be coherent with rainfall fluctuations). The impact of the Kelvin wave appears clearly through weak precipitation when its dry phase is present on 3 July, then an abrupt rainfall increase on 6 and 7 July at the maximum of its wet phase, followed by weaker rainfall amounts once the wet phase goes farther east.

6. Discussion and conclusions

The dominant mode of convectively coupled Kelvin waves has been detected over the Atlantic and West Africa. When detected, these propagate eastward as a single wave packet, as opposed to a wave train. The waves affecting Africa tend to initiate over the eastern Pacific sector, interact with deep convection of the marine ITCZ over the Atlantic and of the continental ITCZ over West and central Africa, then weaken over East Africa and the Indian Ocean. Over the Atlantic and Africa, their mean kinematic characteristics are a wavelength of 8000 km and a phase speed of 15 m s^{-1}, leading to a period of 6–7 days. This corresponds to an equivalent depth of 25 m for a theoretical dry Kelvin wave. The African Kelvin wave activity shows a pronounced seasonal cycle, with most activity outside of northern summer when the ITCZ is close to the equator, facilitating the interactions between convection and these equatorially trapped waves. They can modulate the life cycle and track of individual MCSs. As their wavelength is long, strong Kelvin waves appear to be able to strengthen or break up the ITCZ over the whole West African domain.

The convective and dynamical patterns identified over the Atlantic and Africa have some resemblance with theoretical equatorially trapped Kelvin wave solution on an equatorial β plane. The passage of the wave is preceded at low levels by easterly and followed by westerly wind anomalies, partly in phase with negative and positive geopotential perturbations, respectively, the whole structure propagating at the same speed. Near the coast of West Africa, near-surface westerly anomaly winds appear to contribute to enhance convection in the ITCZ via enhanced moisture advection and are associated with the negative OLR anomalies, while easterly anomalies contribute to weaken convection and precede the occurrence of following negative OLR anomalies by about two days. Most of the flow is in the zonal direction as predicted by theory, and there is a tendency for the dynamical fields to be symmetric about the equator, although the strong monsoonal heating over West Africa and the convection in the ITCZ concentrated well north of the equator (about 10°N at the full development of the African monsoon) favors meridional southerly inflow. This Kelvin wave structure, where the symmetric dynamical fields and the asymmetric convection interact to sustain the simultaneous eastward propagation of both fields, has also been observed over the eastern Pacific during northern summer. However the effect of strong heating over the African continent during the monsoon season results in a modification of the expected vertical Kelvin wave structure, which is not so easy to explain. In the upper troposphere and the stratosphere, within and slightly ahead of the region of deep upward motion, the temperature contours slope sharply eastward with height, as expected from an eastward-moving heat source that forces a dry Kelvin response. The stratospheric signal is consistent with a vertically propagating Kelvin wave with eastward and downward phase and upward energy propagation, forced from below by the deep convective heating. In the troposphere, the quadrature arrangement between vertical motion and temperature, a warm

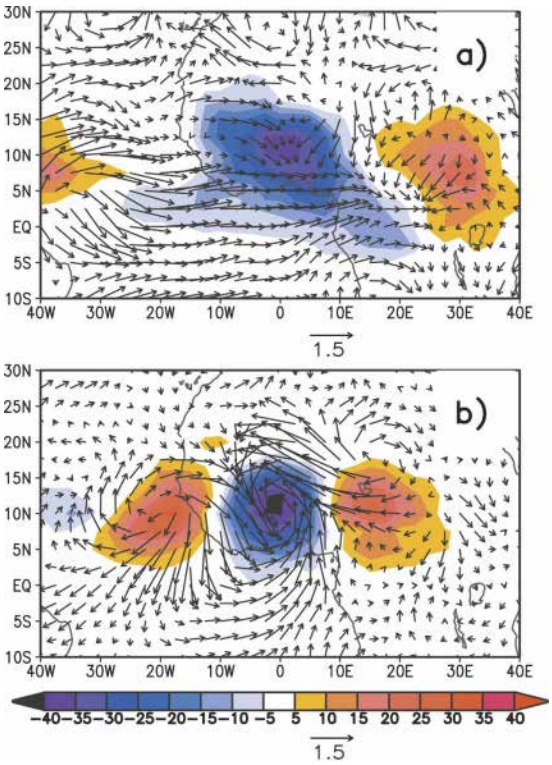

FIG. 10. (a) Composite fields of wet-minus-dry Kelvin phases based on the Kelvin wave index on the period June–September 1979–2000. From this standardized index time series, we retained the dates (called t_0) where it is maximum (minimum) and greater (lower) than 1.5 to define a dry (wet) Kelvin phase. Nonfiltered OLR (shaded; W m^{-2}) and nonfiltered 925-hPa wind (vectors) are displayed. Vector scale (m s^{-1}) is displayed below. (b) Same as in (a), but based on the TD-filtered index.

(cold) temperature anomaly leading (following) the upward motion, is close to the dry Kelvin wave pattern, apart from the fact that there is no clear westward tilt with height below 250 hPa, as observed over the Pacific and Indian oceanic basins. At 20°W no tilt is evident, while at 0° longitude some westward tilt is present but with a not-so-well-organized pattern.

The impact of the synoptic-scale Kelvin wave on convection in the West African monsoon can be compared to the impact of the well-known African easterly waves. We computed an index to estimate the easterly wave activity in the African ITCZ by averaging TD-filtered OLR values (Fig. 1) over the ITCZ area 7.5°–12.5°N, 10°W–10°E. This approach is a bit different from the analysis of the Kelvin wave since we do not perform EOF decomposition of the TD signal but used the TD-filtered signal as a whole. We show in Fig. 3 through a wavelet diagram that the TD index has a high seasonal evolution with its highest energy between July and August and that it is centered around a periodicity of 3 and 5 days. Figure 10 compares the composite field of wet-minus-Kelvin phases based on the Kelvin wave index (Fig. 10a) with the one based on the TD index (Fig. 10b), for nonfiltered OLR and 925-hPa wind. The composite pattern for the Kelvin signal has already been described in the previous sections. The TD pattern has been computed with the same process: the wet (dry) cases have been selected when the standardized TD index is minimum (maximum) and weaker (higher) than minus (plus) 1.5. This pattern shows very clearly the signal of the African easterly waves even though they develop mainly at 700 hPa. Easterly waves significantly modulate convection in the African ITCZ by enhancing convection in the northerly wind sector ahead of the wave and in the trough of the wave, whereas convection is weakened in the ridge. This pattern is very consistent and in close agreement with the results of Kiladis et al. (2006). The spatial extent of OLR anomalies related to Kelvin waves is wider than for OLR anomalies related to an easterly wave and the range of the OLR anomaly is similar, being a bit higher for the easterly wave. We see also that Kelvin waves can impact convection over central and East Africa, which is not the case for easterly waves, which modulate convection mainly west of 10°E (Diedhiou et al. 1999).

We note that the composite method that we have used is based on a reference point at fixed longitudes, which highlights less of the signal in remote areas. This is due to the spread in the individual composite members as one moves farther from the reference point. However, the fact that we computed EOF fields on ca domain larger than West and central Africa has enabled us to produce highly structured spatial patterns that are less artificially localized over tropical Africa. Another advantage of this EOF approach is to be able to extract the main mode of the Kelvin wave, providing more consistent atmospheric patterns than when these waves are detected by using the whole Kelvin-filtered signal contained in the box of Fig. 1 (not shown).

In the analysis of the African monsoon and the Atlantic marine ITCZ, it is impossible to ignore the Kelvin wave as one of the main synoptic-scale weather systems, which plays a comparable role as African easterly waves for modulating convection. Its detection over the tropical Atlantic is necessary for local meteorologists to improve their forecasts over West and central Africa. The intensive field experiment of the African Monsoon Multidisciplinary Analyses (AMMA) program during the summer monsoon of 2006 provides an ideal test bed for such an issue.

Acknowledgments. We are grateful to the NOAA–CIRES Climate Diagnostics Center (Boulder, Colora-

do) for providing the NCEP–NCAR reanalysis dataset and the Interpolated OLR dataset from their Web site (http://www.cdc.noaa.gov/). We thank also Henri Laurent (LTHE, IRD) for providing the daily rainfall dataset and the cloud cluster dataset. We also warmly thank the three reviewers who provided us with a very detailed examination of our draft. GNK was supported by NOAA's Climate Program Office under Grant GC05-156. Based on French initiative, AMMA was built by an international scientific group and is currently funded by a large number of agencies, especially from France, the United Kingdom, the United States, and Africa. It has been the beneficiary of a major financial contribution from the European Community's Sixth Framework Research Programme. Detailed information on scientific coordination and funding is available on the AMMA International Web site (http://www.amma-international.org).

REFERENCES

Arkin, P. A., 1979: The relationship between fractional coverage of high cloud and rainfall accumulations during GATE over the B-scale array. *Mon. Wea. Rev.,* **107,** 1382–1387.

Cattell, R. B., 1966: The scree test for the number of factors. *Multivariate Behav. Res.,* **1,** 245–276.

Diedhiou, A. S., S. Janicot, A. Viltard, P. de Felice, and H. Laurent, 1999: Easterly wave regimes and associated convection over West Africa and tropical Atlantic: Results from NCEP/NCAR and ECMWF reanalysis. *Climate Dyn.,* **15,** 795–822.

Duvel, J. P., 1989: Convection over tropical Africa and the Atlantic Ocean during northern summer. Part I: Interannual and diurnal variations. *Mon. Wea. Rev.,* **117,** 2782–2799.

——, 1990: Convection over tropical Africa and the Atlantic Ocean during northern summer. Part II: Modulation by easterly waves. *Mon. Wea. Rev.,* **118,** 1855–1868.

Folland, C. K., T. N. Palmer, and D. E. Parker, 1986: Sahel rainfall and worldwide sea temperature 1901–1985. *Nature,* **320,** 602–607.

Grist, J. P., and S. E. Nicholson, 2001: A study of the dynamic factors influencing the rainfall variability in the West African Sahel. *J. Climate,* **14,** 1337–1359.

Grodsky, S. A., and J. A. Carton, 2001: Coupled land/atmosphere interactions in the West African monsoon. *Geophys. Res. Lett.,* **28,** 1503–1506.

——, ——, and S. Nigam, 2003: Near surface westerly wind jet in the Atlantic ITCZ. *Geophys. Res. Lett.,* **30,** 2009, doi:10.1029/2003GL017867.

Gruber, A., 1974: The wavenumber–frequency spectra of satellite-measured brightness in the Tropics. *J. Atmos. Sci.,* **31,** 1675–1680.

——, and A. F. Krueger, 1974: The status of the NOAA outgoing longwave radiation data set. *Bull. Amer. Meteor. Soc,* **65,** 958–962.

Hall, N. M. J., G. N. Kiladis, and C. D. Thorncroft, 2006: Three-dimensional structure and dynamics of African easterly waves. Part II: Dynamical modes. *J. Atmos. Sci.,* **63,** 2231–2245.

Hastenrath, S., 1995: *Climate Dynamics of the Tropics.* Kluwer Academic, 488 pp.

Hodges, K. I., and C. D. Thorncroft, 1997: Distribution and statistics of African mesoscale convective weather systems based on the ISCCP Meteosat imagery. *Mon. Wea. Rev.,* **125,** 2821–2837.

Janicot, S., and B. Sultan, 2001: Intra-seasonal modulation of convection in the West African monsoon. *Geophys. Res. Lett.,* **28,** 523–526.

——, S. Trzaska, and I. Poccard, 2001: Summer Sahel-ENSO teleconnection and decadal time scale SST variations. *Climate Dyn.,* **18,** 303–320.

Kalnay, E., and Coauthors, 1996: The NCEP/NCAR 40-Year Reanalysis Project. *Bull. Amer. Meteor. Soc.,* **77,** 437–471.

Kanamitsu, M., W. Ebisuzaki, J. Woollen, S.-K. Yarg, J. J. Hnilo, M. Fiorino, and G. L. Potter, 2002: NCEP–DOE AMIP-II reanalysis (R-2). *Bull. Amer. Meteor. Soc,* **83,** 1631–1643.

Kiladis, G. N., and K. M. Weickmann, 1997: Horizontal structure and seasonality of large-scale circulations associated with submonthly tropical convection. *Mon. Wea. Rev.,* **125,** 1997–2013.

——, C. D. Thorncroft, and N. M. J. Hall, 2006: Three-dimensional structure and dynamics of African easterly waves. Part I: Observations. *J. Atmos. Sci.,* **63,** 2212–2230.

Laing, A. G., and J. M. Fritsch, 1993: Mesoscale convective complexes in Africa. *Mon. Wea. Rev.,* **121,** 2254–2263.

——, and ——, 1997: The global population of mesoscale convective complexes. *Quart. J. Roy. Meteor. Soc.,* **123,** 389–405.

Lamb, P. J., 1978a: Large scale tropical surface circulation patterns associated with Subsaharan weather anomalies. *Tellus,* **30,** 240–251.

——, 1978b: Case studies of tropical Atlantic surface circulation patterns during recent sub-Saharan weather anomalies: 1967 and 1968. *Mon. Wea. Rev.,* **106,** 482–491.

Liebmann, B., and C. A. Smith, 1996: Description of a complete (interpolated) outgoing longwave radiation dataset. *Bull. Amer. Meteor. Soc.,* **77,** 1275–1277.

Mathon, V., and H. Laurent, 2001: Life cycle of Sahelian mesoscale convective cloud systems. *Quart. J. Roy. Meteor. Soc.,* **127,** 377–406.

——, ——, and T. Lebel, 2002: Mesoscale convective systems rainfall in the Sahel. *J. Appl. Meteor.,* **41,** 1081–1092.

Matsuno, T., 1966: Quasi-geostrophic motion in the equatorial area. *J. Meteor. Soc. Japan,* **44,** 25–42.

Matthews, M., 2004: Intraseasonal variability over tropical Africa during northern summer. *J. Climate,* **17,** 2427–2440.

Mekonnen, A., 2006: The role of Kelvin wave activity on convection and rainfall over tropical Africa. Preprints, *27th Conf. on Hurricanes and Tropical Meteorology,* Monterey, CA, Amer. Meteor. Soc., 23–28.

Mounier, F., and S. Janicot, 2004: Evidence of two independent modes of convection at intraseasonal timescale in the West African summer monsoon. *Geophys. Res. Lett.,* **31,** L16116, doi:10.1029/2004GL020665.

Newell, R. E., and J. E. Kidson, 1984: African mean wind changes between Sahelian wet and dry periods. *J. Climatol.,* **4,** 27–33.

North, G. R., T. L. Bell, R. F. Cahalan, and F. J. Moeng, 1982: Sampling errors in the estimation of empirical orthogonal function. *Mon. Wea. Rev.,* **110,** 699–706.

Pires, P., J.-L. Redelsperger, and J.-P. Lafore, 1997: Equatorial atmospheric waves and their association to convection. *Mon. Wea. Rev.,* **125,** 1167–1184.

Reed, R. J., D. C. Norquist, and E. E. Recker, 1977: The structure

and properties of African wave disturbances as observed during Phase III of GATE. *Mon. Wea. Rev.,* **105,** 317–333.

Richman, M. B., 1986: Rotation on principal component. *J. Climatol.,* **6,** 293–335.

Roundy, P. E., and W. M. Frank, 2004: A climatology of waves in the equatorial region. *J. Atmos. Sci.,* **61,** 2105–2132.

Rowell, D. P., 2001: Teleconnections between the tropical Pacific and the Sahel. *Quart. J. Roy. Meteor. Soc,* **127,** 1683–1706.

——, C. K. Folland, K. Maskell, and M. N. Ward, 1995: Variability of summer rainfall over tropical North Africa (1906–1992): Observations and modelling. *Quart. J. Roy. Meteor. Soc.,* **121,** 669–704.

Straub, K. H., and G. N. Kiladis, 2002: Observations of a convectively coupled Kelvin wave in the eastern Pacific ITCZ. *J. Atmos. Sci.,* **59,** 30–53.

——, and ——, 2003: The observed structure of convectively coupled Kelvin waves: Comparison with simple models of coupled wave instability. *J. Atmos. Sci.,* **60,** 1655–1668.

Sultan, B., and S. Janicot, 2003: The West African monsoon dynamics. Part II: The "preonset" and "onset" of the summer monsoon. *J. Climate,* **16,** 3407–3427.

——, ——, and A. Diedhiou, 2003: The West African monsoon dynamics. Part I: Documentation of intraseasonal variability. *J. Climate,* **16,** 3389–3406.

Takayabu, Y., 1994: Large-scale cloud disturbances associated with equatorial waves. Part I: Spectral features of the cloud disturbances. *J. Meteor. Soc. Japan,* **72,** 433–449.

Thompson, R. M., S. W. Payne, E. E. Recker, and R. J. Reed, 1979: Structure and properties of synoptic-scale wave disturbances in the intertropical convergence zone of the eastern Atlantic. *J. Atmos. Sci.,* **36,** 53–72.

Thorncroft, C. D., and B. J. Hoskins, 1994a: An idealized study of African easterly waves. Part I: A linear view. *Quart. J. Roy. Meteor. Soc.,* **120,** 953–982.

——, and ——, 1994b: An idealized study of African easterly waves. Part II: A nonlinear view. *Quart. J. Roy. Meteor. Soc.,* **120,** 983–1015.

Torrence, C., and G. P. Compo, 1998: A practical guide to wavelet analysis. *Bull. Amer. Meteor. Soc.,* **79,** 61–78.

Wang, H., and R. Fu, 2007: The influence of Amazon rainfall on the Atlantic ITCZ through convectively coupled Kelvin waves. *J. Climate,* **20,** 1188–1201.

Ward, M. N., 1998: Diagnosis and short-lead time prediction of summer rainfall in tropical North Africa at interannual and multidecadal timescales. *J. Climate,* **11,** 3167–3191.

Wheeler, M., and G. N. Kiladis, 1999: Convectively coupled equatorial waves: Analysis of clouds and temperature in the wavenumber–frequency domain. *J. Atmos. Sci.,* **56,** 374–399.

——, ——, and P. J. Webster, 2000: Large-scale dynamical fields associated with convectively coupled equatorial waves. *J. Atmos. Sci.,* **57,** 613–640.

Zangvil, A., 1975: Temporal and spatial behavior of large-scale disturbances in tropical cloudiness deduced from satellite brightness data. *Mon. Wea. Rev.,* **103,** 904–920.

Zhang, C., and P. J. Webster, 1989: Effects of zonal flows on equatorially trapped waves. *J. Atmos. Sci.,* **46,** 3632–3652.